Nanoscale

PAPER

CrossMark
← click for updates

Refractive index sensing with Fano resonant plasmonic nanostructures: a symmetry based nonlinear approach†

Jérémy Butet* and Olivier J. F. Martin*

Sensing using surface plasmon resonances is one of the most promising practical applications of plasmonic nanostructures and Fano resonances allow achieving a lower detection limit thanks to their narrow spectral features. However, a narrow spectral width of the subradiant mode in a plasmonic system, as observed in the weak coupling regime, is in general associated with a low modulation of the complete spectral response. In this article, we show that this limitation can be overcome by a nonlinear approach based on second harmonic generation and its dependence on symmetry at the nanoscale. The Fano resonant systems considered in this work are gold nanodolmens. Their linear and nonlinear responses are evaluated using a surface integral equation method. The numerical results demonstrate that a variation of the refractive index of the surrounding medium modifies the coupling between the dark and bright modes, resulting in a modification of the electromagnetic wave scattered at the second harmonic wavelength, especially the symmetry of the nonlinear emission. Reciprocally, we show that evaluating the asymmetry of the nonlinear emission provides a direct measurement of the gold nanodolmens dielectric environment. Interestingly, the influence of the refractive index of the surrounding medium on the nonlinear asymmetry parameter is approximately 10 times stronger than on the spectral position of the surface plasmon resonance: hence, smaller refractive index changes can be detected with this new approach. Practical details for an experimental realization of this sensing scheme are discussed and the resolution is estimated to be as low as $\Delta n = 1.5 \times 10^{-3}$, respectively 1.5×10^{-5}, for an acquisition time of 60 s for an isolated gold nanodolmen, respectively an array of 10×10 nanodolmens.

1. Introduction

The optical properties of plasmonic nanostructures have been widely studied due to their potential new applications in the field of nanophotonics.[1,2] Indeed, the collective oscillations of the conduction electrons, the surface plasmon resonances, result in a strong enhancement of the scattering and absorption cross sections, as well as localization of light far below the diffraction limit.[3,4] The coupling and hybridization between plasmonic modes enables further tailoring and controlling the optical properties of metallic nanostructures for specific applications.[5–9] Hence, surface plasmon resonances are versatile sensing tools since their width and position depend on the size, shape, composition and dielectric constant of the surrounding medium.[10] This latter dependence opens the way to one of the most promising use of metallic nanoparticles:

sensing using localized surface plasmon resonances (LSPR).[11–13] Sensors based on this principle are able to detect small changes in the vicinity of plasmonic structures through monitoring of the LSPR spectral position shift. Recently, significant attention was paid in that context to plasmonic nanostructures supporting Fano resonances due to their unusual electromagnetic response, which includes narrow optical features.[14–16] Fano resonances have been reported in various plasmonic systems, including gratings,[17,18] asymmetric nanodimers,[19,20] ring-disk nanocavities,[21–23] dolmens,[24–26] and plasmonic oligomers.[27–30] Several formalisms were developed to describe Fano resonances and their characteristic asymmetric lineshape in terms of coupling between optical dark (subradiant) and bright (superradiant) modes.[31–34] It was also shown that Fano resonances arising from the coupling between bright modes only can be observed in the scattering spectra of specific nanostructures.[34–38] In some specific plasmonic Fano systems, the interaction between bright and dark modes can also lead to a window of transparency similar to the electromagnetically induced transparency observed in atomic physics.[39,40] Because of their narrower spectral width compared to conventional plasmon resonances and larger induced field enhancement,

*Nanophotonics and Metrology Laboratory (NAM), Swiss Federal Institute of Technology Lausanne (EPFL), 1015 Lausanne, Switzerland.
E-mail: jeremy.butet@epfl.ch, olivier.martin@epfl.ch*
†Electronic supplementary information (ESI) available. See DOI: 10.1039/c4nr05623j

Fano resonances have been used for a variety of applications including plasmonic rulers[41,42] and biosensors.[23,43–46] Note that it is important to control the coupling regime for the optimization of such applications.[42] Indeed, it was recently demonstrated that the Fano system should be used in the weak coupling regime in order to enhance the influence of the dielectric environment on its lineshape.[42,45] However, a narrow spectral width (corresponding to weak radiative losses) of the subradiant mode is associated with a low modulation of the complete spectral response and is difficult to observe in scattering spectra.[45] As a consequence, new approaches are required to overcome this limitation and to push forward the detection limit of Fano sensors. In this article, we show that a nonlinear readout can provide such an approach.

Over the last decade, a significant effort has been devoted to the study of nonlinear optical processes in plasmonic nanostructures, since LSPR can effectively drive them.[47] Among those different nonlinear optical processes, second harmonic generation (SHG), whereby two photons at the fundamental frequency are converted into one at the second harmonic (SH) frequency, is the simplest and probably the most studied in plasmonic systems.[48–56] The shape dependence of the SH intensity has been investigated for both centrosymmetric and non-centrosymmetric metallic nanostructures, addressing the related symmetry properties in great details.[48–56] Especially, the SHG from gold nanorods, which is the building block of the nanodolmen discussed in this article, has been addressed and the enhancement of the nonlinear response by the LSPR discussed.[57–59] Several studies have reported the observation of SHG from single metallic nanostructures, paving the way for the design of practical applications as nonlinear plasmonic sensing,[60] laser beam characterization,[61,62] sensitive shape characterization,[63–65] and imaging.[66–68] For practical applications, it is also important to increase the nonlinear conversion at the nanoscale and multiresonant plasmonic nanostructures, as well as Fano resonant nanostructures, were found to be efficient to do so.[69–72] Recently, we have shown that the combination of the intrinsic properties of Fano resonances with SHG enable the design of nonlinear plasmonic nanorulers with very high sensitivity.[73]

In this article, we theoretically investigate the remote detection of refractive index changes using the SH response of gold nanodolmens which support Fano resonances. The linear case is addressed first in order to demonstrate the benefit of a nonlinear approach for the readout of Fano sensors; the SHG is considered next. Although the modulation depth is not dramatically increased in the nonlinear response, we will show that the symmetry of the nonlinear response can be exploited to enhance sensitivity. Indeed, the presented numerical results clearly demonstrate that a variation of the refractive index of the surrounding medium modifies the symmetry of the electromagnetic wave scattered at the SH wavelength. This phenomenon is explained by the modification of the coupling between the dark and bright modes supported by the different parts of the gold nanodolmens. When the refractive index of the surrounding medium changes, the influence on the asymmetry of the nonlinear response is much stronger than on the linear LSPR spectral position.

2. Numerical method

The linear optical responses have been calculated using a surface integral formulation. A plane wave excitation is considered throughout. The dielectric constant for gold is taken from experimental data at both the fundamental and second harmonic wavelengths.[74] For the SHG computations, the linear surface currents, which are expanded on Rao–Wilton–Glisson (RWG) basis functions,[75,76] are used for the evaluation of the fundamental electric fields just below the gold surfaces and then used for the calculation of the surface SH polarization. Only the component $\chi_{surf,nnn}$ of the nonlinear susceptibility surface tensor, where n denotes the component normal to the surface, is considered since recent experimental results indicate that this term dominates the surface response of metallic nanoparticles.[77,78] Note that other contributions to the SH signal, namely the component $\chi_{surf,ttn}$ of the surface tensor (where t denotes the component tangential to the surface) and bulk contribution, are theoretically allowed but these terms contribute only weakly to the total SH wave.[77,78] In the spectral range considered in this work, the wavelength dependence of the nonlinear polarization is expected to be weak and the tensor element $\chi_{surf,nnn} = 1$ for all the numerical results reported in this article.[77,78] The SH surface currents are obtained solving the SIE formulation taking into account the nonlinear polarization and enforcing the boundary conditions at the nanostructures surfaces.[79] The SH surface currents are expanded like the linear surface currents on RWG basis functions and the expanding coefficients are found by applying the method of moments with Galerkin's testing.[75,76] A Poggio-Miller-Chang-Harrington-Wu formulation is used to ensure accurate solutions even at resonant conditions.[75,76] The SH electric field is then deduced from the SH surface currents using a two-term subtraction method for the evaluation of the Green's functions.[75] The mesh is composed of 2376 triangles (see Fig. 1).
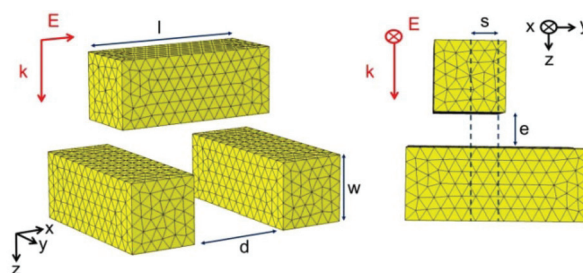

Fig. 1 Schematic of the gold nanodolmen studied in this work. The parameters are fixed to the following values: d = 60 nm, w = 40 nm, l = 100 nm, and e = 20 nm. The value of the parameter s is modified through the manuscript and mentioned in the different figure captions. For this figure, the parameter s is set to 15 nm. The mesh is composed of 2376 triangles.

3. Results and discussion

3.1 Linear optical response

The Fano resonant system discussed in this article is shown in Fig. 1 where the different geometrical parameters are introduced. The considered nanostructure is composed of three gold nanorods: one of the gold nanorod is placed on top of the two other nanorods. The three nanorods are identical (100 nm long and their width w is 40 nm). The separation between the two parallel nanorods d is 60 nm. This gold nanodolmen is excited by an incident plane wave as shown in Fig. 1. The top nanorod supports a dipolar plasmonic mode which is strongly coupled to the incoming plane wave and is able to efficiently radiate light to the far-field. On the contrary, the two bottom parallel nanorods support a quadrupolar plasmonic mode.[40] The out of phase dipole moments supported by each parallel nanorod prevent this quadrupolar mode from efficiently radiating light to the far-field. As a consequence, the quadrupolar mode cannot be excited by the homogeneous field of the incoming plane wave. The backward scattered intensity in the linear regime is computed as a function of the incident wavelength for different values of the symmetry breaking parameter s, assuming a surrounding medium with refractive index $n = 1.33$, corresponding to a nanodolmen in water (solid lines in Fig. 2). In the symmetric case, when $s = 0$ and the top bar is situated exactly at the center of the two parallel nanorods, a strong enhancement of the backward scattered intensity is observed at 780 nm, corresponding to the resonant excitation of the dipolar mode supported by the top nanorod.[42] Indeed, the coupling between the dipolar and the quadrupolar modes vanishes in the symmetric case and only the dipolar mode is excited by the incoming plane wave. As the asymmetry of the nanostructure increases, the optical response of the dolmen

nanostructure evolves from a single Lorentzian resonance to a Fano-like lineshape.[40,42] The asymmetric spectral response resulting from the coupling between the dipolar and the quadrupolar modes evolves with the symmetry parameter s.[42,72] Further computations have been performed considering a higher value of the refractive index for the surrounding medium, $n = 1.37$ (shown as dashed lines in Fig. 2). For all the coupling regimes, a clear redshift of the Fano resonance is observed when the background refractive index changes from $n = 1.33$ to 1.37. The dip in the Fano resonance is shifted by 22 nm, corresponding to a sensitivity of 550 nm per refractive index unit (RIU). On the contrary, the influence of the background on the modulation depth is negligible. Indeed, since the dark and the bright modes have both their field equally present in the environment, their sensitivity is similar *i.e.* they are shifted by the same amount and the overall shape of the spectral response of the system does not change, as discussed by B. Gallinet *et al.*[45] It was reported that Fano plasmonic sensing is more efficient in the weak coupling when the spectral width of the dark mode is limited only by ohmic losses. Nevertheless, a narrow spectral width of the subradiant mode is in general associated with a low modulation of the complete spectral response.[45] In the following, we will show how to overcome this limitation by considering the nonlinear optical response of the gold nanodolmens, instead of their linear response.

3.2 Second harmonic generation

Let us now consider the SH optical response of a gold nanodolmen for different backgrounds. It is well known that SHG is forbidden in the bulk of centrosymmetric media within the electric dipole approximation.[80] However, this symmetry is broken at the interface between two centrosymmetric media
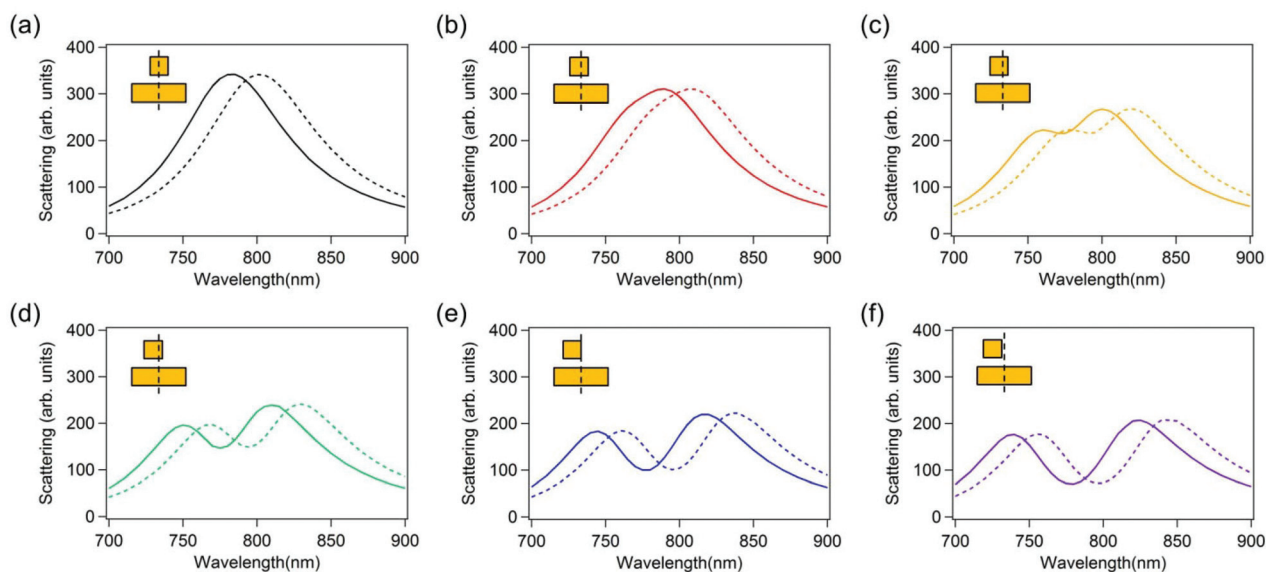

Fig. 2 Backward scattered intensity from a gold nanodolmen as a function of the incident wavelength computed for different values of the symmetry parameter s: (a) $s = 0$ nm, (b) $s = 5$ nm, (c) $s = 10$ nm, (d) $s = 15$ nm, (e) $s = 20$ nm, and (f) $s = 25$ nm. The refractive index of the surrounding medium is $n = 1.33$ (solid lines) and $n = 1.37$ (dashed lines), respectively.

and SHG can originate from metallic nanostructure surfaces.[80] Surface integral equations methods only require the discretization of the surfaces of the metal nanostructures, exactly where the SHG sources are located, and are therefore extremely well suited for accurate SHG computations.[75] Fig. 3 shows the SH intensity from a gold nanodolmen for different values of the parameter s. The SH intensity has been integrated over a sphere with radius $r = 50$ μm. Contrary to the linear scattering, which corresponds to the excitation of an electric dipole mode, SHG involves higher emission modes resulting in a SH wave scattered in several directions.[56] Interestingly, the linear and the SH responses exhibit a similar spectral behaviour, compare Fig. 2(a)–(f) and 3(a)–(f). In the symmetric case ($s = 0$ nm, black curves), a Lorentzian function centred at 780 nm ($n = 1.33$) or at 802 nm ($n = 1.37$) is observed. Indeed,

the amplitude of the SH sources standing at the gold nanodolmen surface is directly related to the fundamental near-field intensity. As a consequence, a resonant excitation of the dipolar mode supported by the top nanorod increases the SH signal in the far-field. As previously discussed, the quadrupolar mode supported by the two parallel nanorods is only excited if the symmetry of the nanodolmen is broken ($s \neq 0$).[42,45] In this case, the strength of the SH sources standing at the surface of the two parallel rods increases. Note that the intensity enhancement related to the quadrupolar mode depends on the symmetry parameter s and reaches a maximum value in the intermediate coupling regime.[42] In the asymmetric case, the SH wave does not come only from the top nanorod but nonlinear sources are also present at the two parallel nanorods surfaces, as shown by the SH near-field
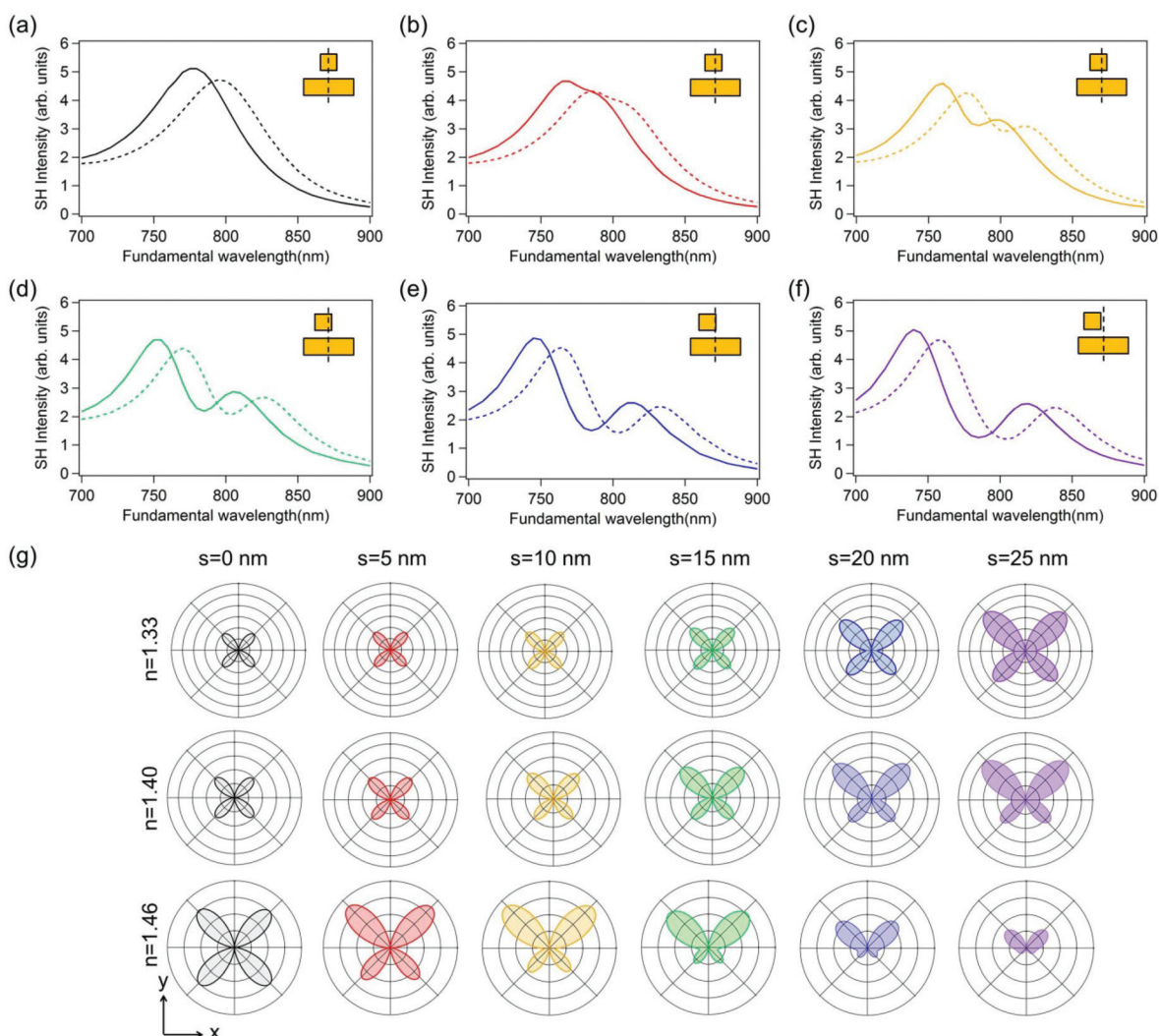

Fig. 3 Total SH intensity from the gold nanodolmen as a function of the incident wavelength computed for different values of the symmetry parameter s: (a) $s = 0$ nm, (b) $s = 5$ nm, (c) $s = 10$ nm, (d) $s = 15$ nm, (e) $s = 20$ nm, and (f) $s = 25$ nm. The refractive index of the surrounding medium is $n = 1.33$ (solid lines) and $n = 1.37$ (dashed lines), respectively. The SH intensity is integrated over a sphere of radius $r = 50$ μm. (g) Normalized SH intensity scattered in the plane containing the two parallel nanorods as a function of the scattering angle considering the SH scattered wave polarized into the scattering plane. The incident wavelength is 860 nm. The refractive index of the surrounding medium $n = 1.33$ (first row), and $n = 1.40$ (second row), and $n = 1.46$ (third row).

intensity maps (Fig. 4).[73] Despite this more complex nonlinear sources distribution, the total SH intensity follows the trend of the linear scattering for the different symmetry parameters s (compare Fig. 2 and 3). When the refractive index of the surrounding medium increases, the maximum of the SH intensity is redshifted following the behaviour of the Fano resonance observed previously in the linear regime (Fig. 2). Since the total SH intensity is strongly correlated to the Fano resonance wavelength, their sensitivities to changes of the surrounding medium refractive index are identical. Furthermore, the linear and the nonlinear lineshapes are also similar and the benefit of a nonlinear approach for plasmonic sensing seems to be rather limited when measuring the entire SH intensity. It is however very difficult to experimentally measure the total SH

intensity and the SH wave is often recorded in a specific scattering plane.[81] In the following, the SH far-field radiation in the plane containing the two parallel nanorods will be investigated in details with the aim of designing sensitive nonlinear Fano sensors. Fig. 3(g) shows for different values of the parameter s the normalized SH intensity scattered in the (O, x, y) plane, which is perpendicular to the incident beam, as a function of the scattering angle, considering the SH scattered wave polarized into this plane.[64] The incident wavelength is set to 860 nm and several values of the refractive index for the surrounding medium n are considered (ranging from $n = 1.33$ to $n = 1.46$). For comparison, the normalized SH intensity scattered in the (O, x, z) plane is shown in the ESI (Fig. S1†). In Fig. 3(g) we observe that the SH emission pattern evolves from a symmetric four-lobe pattern corresponding to a quadrupolar emission for $s = 0$ to asymmetric emission patterns for $s \neq 0$. Indeed, SHG from metallic nanostructures with centrosymmetric shapes is forbidden in the electric dipole approximation, explaining why high multipolar modes are involved in the nonlinear optical response.[82] The angular dependence of the linear scattering was also evaluated, revealing meanly a dipolar nature (see ESI Fig. S2 and S3†). In the case of the symmetric gold nanodolmen ($s = 0$), the SH field is generated by the top nanorod and a SH emission pattern similar to that of a single rod is then expected. For asymmetric nanodolmens, the total SH emission pattern observed in a specific configuration arises from the interference between the SH emissions from the top bar and from the two parallel ones, with their relative weights in the overall signal controlled by the Fano resonance occurring at the fundamental wavelength. Considering a given refractive index n of the surrounding medium, the asymmetry of the SH emission pattern increases as the parameter s increases, i.e. as the coupling between the dipolar and quadrupolar modes at the fundamental wavelength increases. More interestingly, the asymmetry of the SH wave scattered by asymmetric nanodolmens (for which $s \neq 0$) increases as the refractive index of the surrounding medium increases (owing to the modification of the modes coupling) indicating that the symmetry properties of SHG can be used for remote detection. Note that, for a given value of the refractive index of the surrounding medium, the spectral lineshape of the Fano resonance depends on the coupling between the subradiant and the superradiant modes which is controlled by the parameter s. As the refractive index of the surrounding medium increases, the spectral maxima of SHG can be shifted toward or away from the incident wavelength, depending on the parameter s. As a consequence, the SH intensity can decrease or increase as the parameter s evolves, as observed for the 3 rows in Fig. 3(g). In order to quantify the asymmetry of the emission pattern and the influence of the surrounding medium, following the definition introduced in ref. 73, the asymmetry parameter A is computed as:
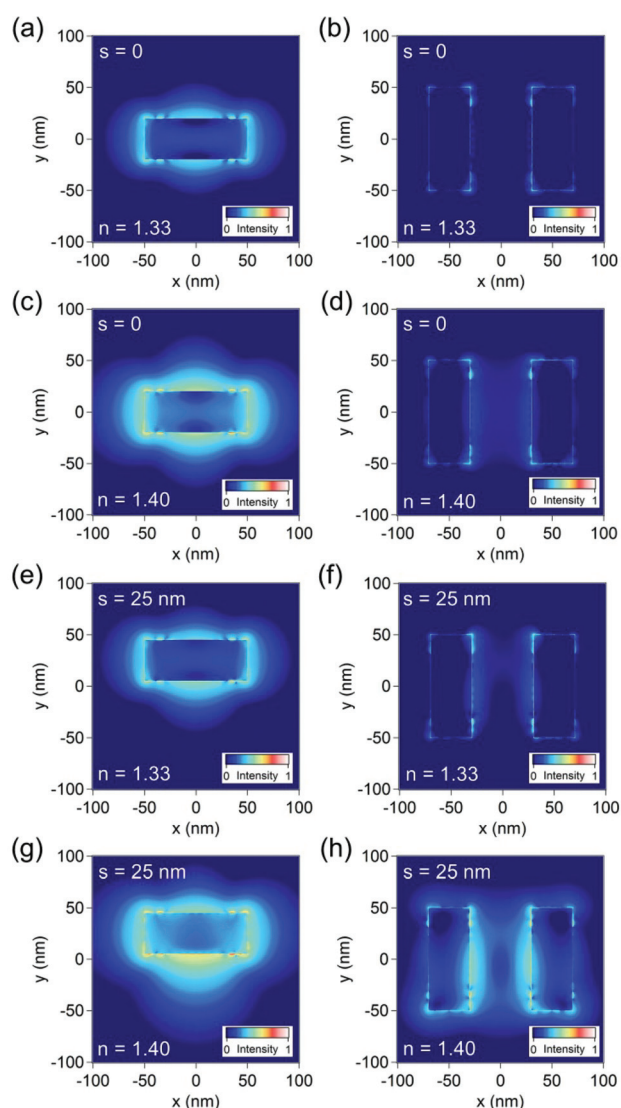

Fig. 4 SH near-field intensity maps (shown in a logarithmic scale) close to (a, c, e, g) the dipolar nanorod antenna and to (b, d, f, h) the two parallel nanorods evaluated for an incident wavelength $\lambda = 860$ nm for different cases: (a–d) $s = 0$ and (e–h) $s = 25$ nm. (a, b, e, f) $n = 1.33$ and (c, d, g, h) $n = 1.40$. The same colorscale is used for the 8 maps.

$$A = \frac{I_1 - I_2}{I_1}, \quad (1)$$

where I_1 and I_2 are the maximal SH intensity scattered in the upper ($y > 0$) and lower ($y < 0$) parts of the polar-plot, respectively. The asymmetry parameter A is reported as a function of the refractive index n for different values of the parameter s in Fig. 5(a). The asymmetry of the linear scattering has also been evaluated following the same approach (dashed lines – Fig. 5(a)) revealing a lower influence of the refractive index. The asymmetry parameter A for SHG evolves from 0 for a symmetric emission pattern for $s = 0$ to almost 80% for the highest values of the symmetry parameter s and of the refractive index n. The asymmetry of the nonlinear emission depends on the coupling between the dark mode and the bright mode and increases with the excitation of the subradiant mode. Independently of the refractive index of the surrounding medium, this subradiant mode is not excited in the symmetric configuration ($s = 0$), explaining that the asymmetry parameter A vanishes in this case (Fig. 5). On the contrary, the asymmetry increases with the refractive index n even for a minute symmetry breaking ($s = 5$ nm – red curve). In the strong coupling regime ($s = 25$ nm), a modification of the refractive index by 0.1 RIU results in a variation of the asymmetry parameter A as high as

40%. For example, when the refractive index of the surrounding medium increases from 1.37 to 1.46, the asymmetry parameter A evolves from 31.5% to 68.3%, *i.e.* is multiplied by more than 2. In the intermediate coupling regime ($s = 10$ nm), the asymmetry parameter A evolves from 16.5% to 49% (corresponding to a multiplication by 3 and an absolute change of 32.5%) when the refractive index of the surrounding medium increases from 1.37 to 1.46. Very similar sensing performances are obtained in the different coupling regimes (except for the non-coupled case) emphasizing the flexibility of a nonlinear approach for the readout of Fano sensors.

3.3 Comparison with the classical linear readout

In this section, the symmetry based nonlinear approach for plasmonic sensing is compared with the classical linear approach. The most important parameter for determining sensing performance is the sensitivity, *i.e.* the amplitude of the output parameter variation (the asymmetry of the SH response for the nonlinear case or the LSPR spectral position for the linear case) for a given modification of the measured quantity (the refractive index of the surrounding medium in the present case). In order to make the comparison between the nonlinear and the linear cases easier, it is necessary to evaluate the variation of both the asymmetry parameter and the spectral position of the LSPR in a similar way. The variation of the asymmetry is computed as:

$$V_A(n) = \frac{|A(n + 0.01) - A(n)|}{A(n)}, \qquad (2)$$

and the variation of the LSPR spectral position is computed as:

$$V_{\lambda_{SPR}}(n) = \frac{|\lambda_{SPR}(n + 0.01) - \lambda_{SPR}(n)|}{\lambda_{SPR}(n)}. \qquad (3)$$

The variation of the LSPR spectral position is computed for $s = 0$ since this parameter does not modify the sensitivity in the linear regime, Fig. 2. Note that the spectral variation of the nonlinear response follows that of the linear scattering. The result is shown in Fig. 5(b) for refractive indexes of the surrounding medium ranging from $n = 1.33$ to 1.49. Note that the asymmetry variation is higher for small values of the parameter s despite smaller absolute variations. This is in agreement with recent observations on the dynamic range provided by Fano resonant structures in the weak coupling regime.[40] Furthermore, the variation of the asymmetry reaches its maximal value at higher refractive indexes n when the parameter s decreases, Fig. 5(b). This is explained by the line-shape of the Fano resonance and the interaction strength between the bright and dark modes in the different coupling regimes (see Fig. 2 and 3). The variation of the asymmetry parameter ranges from 8% to 18% while the variation of the LSPR spectral position remains below 1%. As a consequence, the theoretical detection threshold is much lower when the symmetry properties of SHG are exploited. This emphasizes the benefit of the proposed nonlinear readout, compared to the linear LSPR readout based only on the LSPR shift.
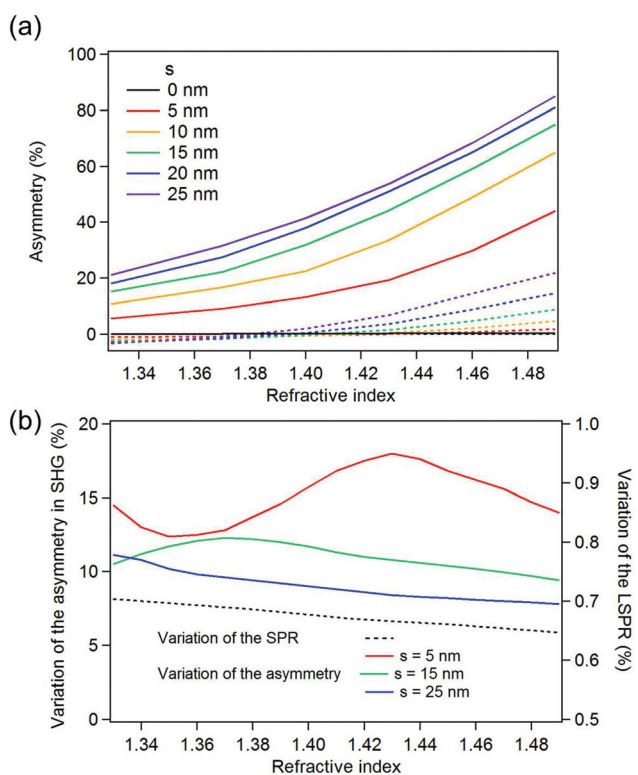

Fig. 5 (a) Asymmetry parameter (as defined by eqn (1)) as a function of the refractive index n evaluated for different values of the parameter s (from 0 nm (black curve) to 25 nm (purple curve)) corresponding to the emission pattern shown in Fig. 3(g). The asymmetry parameters for SHG and linear scattering are shown in full and dashed lines, respectively. The incident wavelength is 860 nm. (b) Variation of the asymmetry (left axis – eqn (2)) and of the LSPR spectral position (right axis – eqn (3)) as a function of the refractive index. The variation of the LSPR spectral position is computed for $s = 0$. The variations of the SHG and of the linear scattering are shown in full and dashed lines, respectively.

3.4 Experimental implementation

Let us briefly discuss some implementation details for the proposed SH sensing scheme and use published experimental data to estimate the sensitivity that could be achieved with nanodolmens. SHG is a nonlinear optical process that requires the use of pulsed laser systems. The SHG from a single 150 nm gold nanoparticle embedded in a transparent matrix was recently observed using the combination of a femtosecond laser (pulse duration ~180 fs and pulse energy ~10 nJ) and a very sensitive gated photon counting systems with typical acquisition time of 10 seconds.[51,83] The SH signal coming from the homogeneous medium, corresponding to the background, is very low due to the properties of SHG.[51,83] In this case, the signal-to-noise ratio is given by the square root of the number of counts. In these previously reported experiments, the count rate was 10 counts s^{-1} for a single 150 nm gold nanoparticle. To estimate the corresponding figure for an experiment based on the nanodolmens proposed here, we have first performed computations for a gold nanosphere with a 150 nm diameter; the results show that the SH signal from the gold nanodolmens is approximately 10 times higher than that of the gold sphere (ESI Fig. S4†). This would correspond to a count rate of 100 counts s^{-1} and a signal-to-noise ratio of 32, respectively 78, for an acquisition time of 10 s, respectively 60 s. In turn, these data correspond to a resolution of $\Delta n = 0.01$, respectively $\Delta n = 10^{-3}$. These values are very good for a plasmonic sensor based on the LSPR of an isolated nanostructure but below the performances of sensing platforms based on propagating surface plasmons (resolution close to $\Delta n = 10^{-7}$).[84–86] However, SHG is a coherent process and the SH response from the nanostructures composing an array can be added up coherently. Considering a 10 × 10 array of gold nanodolmens and an acquisition time of 60 s, the signal-to-noise ratio raises to 7800, corresponding to an estimated resolution $\Delta n = 1.5 \times 10^{-5}$. This value tends to the best resolution reported for a plasmonic sensors based on LSPR ($\Delta n = 2.8 \times 10^{-6}$),[87] supporting the benefit of the approach proposed in this article. Note that the evaluation of the resolution is based on the counts statistics but that a relevant signal treatment could increase the resolution.[88] Furthermore, both the signal-to-noise ratio and the resolution increase with the acquisition time.[89]

The preparation of the plasmonic sensor is an important issue. Advanced nanofabrication techniques such as DNA origami enable the fabrication of 3D rigid gold nanostructures with spatial accuracy down to the nanoscale.[90,91] The addition of a substrate and/or a spacer could modify the nonlinear emission. While method used for the computation of SHG does not enable evaluation of the influence of the substrate and spacer on the asymmetry of the nonlinear emission, the addition of a substrate and/or a spacer does not break the symmetry in the (O, x, y) plane (contrary to the (O, x, z) plane) and the influence on the asymmetry of the nonlinear response is expected to be weak. In addition to the gold nanodolmen fabrication, the surface functionalization is an important issue for biomolecular detection.[92,93] It has been widely discussed in the literature and all the different functionalization methods developed for linear plasmonic sensing can be used straightforwardly for nonlinear plasmonic sensors based on symmetry. Furthermore, the interaction between biological analytes and the biorecognition elements could result in asymmetric SH distribution, especially when few analytes are attached to the surface, which could provide further experimental advantages. An optimized distribution of the biorecognition elements on the gold nanodolmens (for example, attached to only one nanorod) could increase the influence on the SH emission and further boost the detection limit.

4. Conclusions

In summary, the detection of refractive index changes using the SH response of gold nanodolmens was theoretically investigated in this work. Even though a nonlinear approach does not dramatically increase the modulation depth recorded for the total SH intensity, the symmetry of the nonlinear response can be exploited for sensing applications. Indeed, the presented numerical results clearly show that a variation of the refractive index of the surrounding medium modifies the symmetry of the electromagnetic wave scattered at the SH wavelength. This phenomenon was explained by the modification of the coupling between the dark and bright modes supported by the gold nanodolmens. In particular, a modification of the refractive index by 0.1 RIU results in a variation of the asymmetry parameter A as high as 18%, indicating the high sensitivity of the proposed nonlinear readout method. For an acquisition time of 60 s, the resolution is evaluated to be $\Delta n = 1.5 \times 10^{-3}$, respectively $\Delta n = 1.5 \times 10^{-5}$, for an isolated gold nanodolmen, respectively an array of 10 × 10 nanodolmens. These results pave the way for the design of efficient plasmonic sensors combining the advantages of Fano resonances and those of nonlinear optical processes, enabling the observation of the adsorption of a very small amount of molecules at nanostructured metal interfaces.[94–97]

Acknowledgements

Notes and references

1 W. L. Barnes, A. Dereux and T. W. Ebbesen, *Nature*, 2003, **424**, 824–830.

2 S. A. Maier, in *Plasmonics: Fundamentals and Applications*, Springer, New York, 2007.

3 J. A. Schuller, E. S. Barnard, W. Cai, Y. Chul Jun, J. S. White and M. L. Brongersma, *Nat. Mater.*, 2010, **9**, 193–204.

4   O. J. F. Martin, C. Girard and A. Dereux, *Phys. Rev. Lett.*, 1995, **74**, 526–529.

5   J. P. Kottmann and O. J. F. Martin, *Opt. Express*, 2001, **8**, 655–663.

6   E. Prodan, C. Radloff, N. J. Halas and P. Nordlander, *Science*, 2003, **302**, 419–422.

7   N. J. Halas, S. Lal, W.-S. Chanq, S. Link and P. Nordlander, *Chem. Rev.*, 2011, **111**, 3913–3961.

8   P. Nordlander, C. Oubre, E. Prodan, K. Li and M. I. Stockman, *Nano Lett.*, 2004, **4**, 899–903.

9   P. K. Jain, W. Huang and M. A. l-Sayed, *Nano Lett.*, 2007, **7**, 2080–2088.

10 L. M. Liz-Marzán, *Langmuir*, 2006, **22**, 32–41.

11 N. Liu, M. L. Tang, M. Hentschel, H. Giessen and A. P. Alivisatos, *Nat. Mater.*, 2011, **10**, 631.

12 J. N. Anker, W. P. Hall, O. Lyandres, N. C. Shah, J. Zhao and R. P. Van Duyne, *Nat. Mater.*, 2008, **7**, 442–452.

13 J. J. Mock, D. R. Smith and S. Schultz, *Nano Lett.*, 2003, **3**, 485–491.

14 B. Luk'yanchuk, N. I. Zheludev, S. A. Maier, N. J. Halas, P. Nordlander, H. Giessen and C. T. Chong, *Nat. Mater.*, 2010, **9**, 707–715.

15 A. E. Miroshnichenko, S. Flach and Y. S. Kivshar, *Rev. Mod. Phys.*, 2010, **82**, 2257–2298.

16 A. B. Khanikaev, C. Wu and G. Shvets, *Nanophotonics*, 2013, **2**, 247–264.

17 A. Christ, Y. Ekinci, H. H. Solak, N. A. Gippius, S. G. Tikhodeev and O. J. F. Martin, *Phys. Rev. B: Condens. Matter*, 2007, **76**, 201405.

18 A. Christ, O. J. F. Martin, Y. Ekinci, N. A. Gippius and S. G. Tikhodeev, *Nano Lett.*, 2008, **8**, 2171–2175.

19 G. Bachelier, I. Russier-Antoine, E. Benichou, C. Jonin, N. Del Fatti, F. Vallée and P.-F. Brevet, *Phys. Rev. Lett.*, 2008, **101**, 197401.

20 A. Lombardi, M. P. Grzelczak, A. Crut, P. Maioli, I. pastoriza-Santos, L. M. Liz-Marzán, N. Del Fatti and F. Vallée, *ACS Nano*, 2013, **7**, 2522–2531.

21 F. Hao, P. Nordlander, Y. Sonnefraud, P. Van Dorpe and S. A. Maier, *ACS Nano*, 2009, **3**, 643–652.

22 Y. H. Fu, J. B. Zhang, Y. F. Yu and B. Luk'yanchuk, *ACS Nano*, 2012, **6**, 5130–5137.

23 A. E. Cetin and H. Altug, *ACS Nano*, 2012, **6**, 9989–9995.

24 C. Wu, A. B. Khanikaev, R. Adato, N. Arju, A. A. Yanik, H. Altug and G. Shvets, *Nat. Mater.*, 2012, **11**, 69–75.

25 N. Verellen, Y. Sonnefraud, H. Sobhani, F. Hao, V. V. Moshchalkov, P. Van Dorpe, P. Nordlander and S. A. Maier, *Nano Lett.*, 2009, **9**, 1663–1667.

26 N. Liu, T. Weiss, M. Mesch, L. Langguth, U. Eigenthaler, M. Hirscher, C. Soennichsen and H. Giessen, *Nano Lett.*, 2010, **10**, 1103–1107.

27 J. A. Fan, C. Wu, K. Bao, J. Bao, R. Bardhan, N. J. Halas, V. N. Manoharan, P. Nordlander, G. Shvets and F. Capasso, *Science*, 2010, **328**, 1135–1138.

28 J. B. Lassiter, H. Sobhani, J. A. Fan, J. Kundu, F. Capasso, P. Nordlander and N. J. Halas, *Nano Lett.*, 2010, **10**, 3184–3189.

29 M. Hentschel, M. Saliba, R. Vogelgesang, H. Giessen, A. P. Alivisatos and N. Liu, *Nano Lett.*, 2010, **10**, 2721–2726.

30 M. Hentschel, D. Dregely, R. Vogelgesang, H. Giessen and N. Liu, *ACS Nano*, 2011, **5**, 2042–2050.

31 B. Gallinet and O. J. F. Martin, *Phys. Rev. B: Condens. Matter*, 2011, **83**, 235427.

32 B. Gallinet and O. J. F. Martin, *ACS Nano*, 2011, **5**, 8999–9008.

33 V. Giannini, Y. Francescato, H. Amrania, C. C. Phillips and S. A. Maier, *Nano Lett.*, 2011, **11**, 2835–2840.

34 M. Rahmani, D. Y. Lei, V. Giannini, B. Lukiyanchuk, M. Ranjbar, T. Y. F. Liew, M. Hong and S. A. Maier, *Nano Lett.*, 2012, **6**, 2101–2106.

35 A. Lovera, B. Gallinet, P. Nordlander and O. J. F. Martin, *ACS Nano*, 2013, **7**, 4527–4536.

36 B. Hopkins, A. N. Poddubny, A. E. Miroshnichenko and Y. S. Kivshar, *Phys. Rev. A*, 2013, **88**, 053819.

37 M. Svendendahl and M. Käll, *ACS Nano*, 2012, **6**, 7533–7539.

38 K. Lodewijks, J. Ryken, W. Van Roy, G. Borghs, L. Lagae and P. Van Dorpe, *Plasmonics*, 2013, **8**, 1379–1385.

39 S. Zhang, D. A. Genov, Y. Wang, M. Liu and X. Zhang, *Phys. Rev. Lett.*, 2008, **101**, 047401.

40 N. Liu, L. Langguth, T. Weiss, J. Kaestel, M. Fleischhauer, T. Pfau and H. Giessen, *Nat. Mater.*, 2009, **8**, 758–762.

41 L. Shao, C. Fang, H. Chen, Y. C. Man, J. Wang and H.-Q. Lin, *Nano Lett.*, 2012, **12**, 1424–1430.

42 B. Gallinet, T. Siegfried, H. Sigg, P. Nordlander and O. J. F. Martin, *Nano Lett.*, 2013, **13**, 497–503.

43 N. Verellen, P. Van Dorpe, C. Huang, K. Lodewijks, G. A. E. Vandenbosch, L. Lagae and V. V. Moshchalkov, *Nano Lett.*, 2011, **11**, 391–397.

44 J. Ye, F. Wen, H. Sobhani, J. B. Lassiter, P. Van Dorpe, P. Nordlander and N. J. Halas, *Nano Lett.*, 2012, **12**, 1660–1667.

45 B. Gallinet and O. J. F. Martin, *ACS Nano*, 2013, **7**, 6978–6987.

46 Y. Zhan, D. Y. Lei, X. Li and S. A. Maier, *Nanoscale*, 2014, **6**, 4705–4715.

47 M. Kauranen and A. V. Zayats, *Nat. Photonics*, 2012, **6**, 737–748.

48 A. Bouhelier, M. Beversluis, A. Hartschuh and L. Novotny, *Phys. Rev. Lett.*, 2003, **90**, 013903.

49 R. C. Jin, J. E. Jureller, H. Y. Kim and N. F. Scherer, *J. Am. Chem. Soc.*, 2005, **127**, 12482–12483.

50 V. K. Valev, N. Smisdom, A. V. Silhanek, B. De Clercq, W. Gillijns, M. Ameloot, V. V. Moshchalkov and T. Verbiest, *Nano Lett.*, 2009, **9**, 3945–3948.

51 J. Butet, J. Duboisset, G. Bachelier, I. Russier-Antoine, E. Benichou, C. Jonin and P.-F. Brevet, *Nano Lett.*, 2010, **10**, 1717–1721.

52 J. Butet, G. Bachelier, I. Russier-Antoine, C. Jonin, E. Benichou and P.-F. Brevet, *Phys. Rev. Lett.*, 2010, **105**, 077401.

53 Y. Zhang, N. K. Grady, C. Ayala-Orozco and N. J. Halas, *Nano Lett.*, 2011, **11**, 5519–5523.

54 H. Husu, R. Siikanen, J. Mäkitalo, J. Lehtolahti, J. Laukkanen, M. Kuittinen and M. Kauranen, *Nano Lett.*, 2012, **12**, 673–677.

55 R. Czaplicki, H. Husu, R. Siikanen, J. Mäkitalo and M. Kauranen, *Phys. Rev. Lett.*, 2013, **110**, 093902.

56 J. Butet, S. Gutta-Dupta and O. J. F. Martin, *Phys. Rev. B: Condens. Matter*, 2014, **89**, 245449.

57 C. Hubert, L. Billot, P.-M. Adam, R. Bachelot, P. Royer, J. Grand, D. Gindre, K. D. Dorhenoo and A. Fort, *Appl. Phys. Lett.*, 2007, **90**, 181105.

58 A. Singh, A. Lehoux, H. Remita, J. Zyss and I. Ledoux-Rak, *J. Phys. Chem. Lett.*, 2013, **4**, 3958–3961.

59 Y. El Harfouch, E. Benichou, F. Bertorelle, I. Russier-Antoine, C. Jonin, N. Lascoux and P.-F. Brevet, *J. Phys. Chem. C*, 2014, **118**, 609–616.

60 J. Butet, I. Russier-Antoine, C. Jonin, N. Lascoux, E. Benichou and P.-F. Brevet, *Nano Lett.*, 2012, **12**, 1697–1701.

61 N. Accanto, J. B. Nieder, L. Piatkowski, M. Castro-Lopez, F. Pastorelli, D. Brinks and N. F. van Hulst, *Light: Sci. Appl.*, 2014, **3**, e143.

62 N. Accanto, L. Piatkowski, J. Renger and N. F. van Hulst, *Nano Lett.*, 2014, **14**, 4078–4082.

63 G. Bautista, M. J. Huttunen, J. Mäkitalo, J. M. Kontio, J. Simonen and M. Kauranen, *Nano Lett.*, 2012, **12**, 3207–3212.

64 J. Butet, K. Thyagarajan and O. J. F. Martin, *Nano Lett.*, 2013, **13**, 1787–1792.

65 C. Sauerbeck, M. Haderlein, B. Schürer, B. Braunschweig, W. Peukert and R. N. K. Taylor, *ACS Nano*, 2014, **8**, 3088–3096.

66 V. K. Valev, A. Volodin, A. V. Silhanek, W. Gillijns, B. De Clercq, Y. Jeyaram, H. Paddubrouskaya, C. G. Biris, N. C. Panoiu, O. A. Aktsipetrov, *et al.*, *ACS Nano*, 2011, **5**, 91–96.

67 V. K. Valev, *Langmuir*, 2012, **28**, 15454–15471.

68 H. Shen, N. Nguyen, D. Gachet, V. Maillard, T. Toury and S. Brasselet, *Opt. Express*, 2013, **21**, 12318–12326.

69 S. I. Bozhevolnyi, J. Beermann and V. Coello, *Phys. Rev. Lett.*, 2003, **90**, 197403.

70 K. Thyagarajan, S. Rivier, A. Lovera and O. J. F. Martin, *Opt. Express*, 2012, **20**, 12860–12865.

71 K. Thyagarajan, J. Butet and O. J. F. Martin, *Nano Lett.*, 2013, **13**, 1847–1851.

72 Y. Zhang, F. Wen, Y. R. Zhen, P. Nordlander and N. J. Halas, *Proc. Natl. Acad. Sci. U. S. A.*, 2013, **110**, 9215–9219.

73 J. Butet and O. J. F. Martin, *ACS Nano*, 2014, **8**, 4931–4939.

74 P. B. Johnson and R. W. Christy, *Phys. Rev. B: Condens. Matter*, 1972, **6**, 4370–4379.

75 A. M. Kern and O. J. F. Martin, *J. Opt. Soc. Am. A*, 2009, **26**, 732–740.

76 J. Mäkitalo, S. Suuriniemi and M. Kauranen, *Opt. Express*, 2011, **19**, 23386–23399.

77 G. Bachelier, J. Butet, I. Russier-Antoine, C. Jonin, E. Benichou and P.-F. Brevet, *Phys. Rev. B: Condens. Matter*, 2010, **82**, 235403.

78 F. X. Wang, F. J. Rodriguez, W. M. Albers, R. Ahorinta, J. E. Sipe and M. Kauranen, *Phys. Rev. B: Condens. Matter*, 2009, **80**, 233402.

79 T. F. Heinz, Second-order nonlinear optical effects at surfaces and interfaces, in *Nonlinear Surface Electromagnetic Phenomena*, ed. H.-E. Ponath and G. I. Stegeman, Elsevier, Amsterdam, 1991.

80 J. E. Sipe, C. Y. So, M. Fukui and G. I. Stegeman, *Phys. Rev. B: Condens. Matter*, 1980, **21**, 4389–4402.

81 B. Schürer, S. Wunderlich, C. Sauerbeck, U. Peschel and W. Peukert, *Phys. Rev. B*, 2010, **82**, 241404.

82 J. I. Dadap, J. Shan, K. B. Eisenthal and T. F. Heinz, *Phys. Rev. Lett.*, 1999, **83**, 4045–4048.

83 J. Butet, G. Bachelier, J. Duboisset, F. Bertorelle, I. Russier-Antoine, C. Jonin, E. Benichou and P.-F. Brevet, *Opt. Express*, 2010, **18**, 22314–22353.

84 J. Homola, in *Surface plasmon resonance based sensors*, Springer-Verlag, Berlin-Heidelberg-New York, 2006.

85 M. Piliarik and J. Homola, *Opt. Express*, 2009, **17**, 16505–16517.

86 S. Patskovsky, M. Vallieres, M. Maisonneuve, I. H. Song, M. Meunier and A. V. Kabashin, *Opt. Express*, 2009, **17**, 2255–2263.

87 K. M. Mayer and J. H. Hafner, *Chem. Rev.*, 2011, **111**, 3828–3857.

88 A. B. Dahlin, J. O. Tegenfeldt and F. Hook, *Anal. Chem.*, 2006, **78**, 4416–4423.

89 J. Duboisset, I. Russier-Antoine, E. Benichou, G. Bachelier, C. Jonin and P.-F. Brevet, *J. Chem. Phys. C*, 2009, **113**, 13477–13481.

90 X. Shen, A. Asenjo-Garcia, Q. Liu, Q. Jiang, F. J. García de Abajo, N. Liu and B. Ding, *Nano Lett.*, 2013, **13**, 2128–2133.

91 X. Shen, P. Zhan, A. Kuzyk, Q. Liu, A. Asenjo-Garcia, H. Zhang, F. J. García de Abajo, A. Govorov, B. Ding and N. Liu, *Nanoscale*, 2014, **6**, 2077–2081.

92 R. A. Sperling and W. J. Parak, *Philos. Trans. R. Soc. London, Ser. A*, 2010, **368**, 1333–1383.

93 R. Subbiah, M. Veerapandian and K. S. Yun, *Curr. Med. Chem.*, 2010, **17**, 4559–4577.

94 C. K. Chen, T. F. Heinz, D. Ricard and Y. R. Shen, *Phys. Rev. Lett.*, 1981, **46**, 1010–1012.

95 D. Heskett, K. J. Song, A. Burns, E. W. Plummer and H.-L. Dai, *J. Chem. Phys.*, 1986, **85**, 7490–7492.

96 O. Dannenberger, M. Buck and M. Grunze, *J. Phys. Chem. C*, 1999, **103**, 2202–2213.

97 W. Gan, G. Gonella, M. Zhang and H.-L. Dai, *J. Chem. Phys.*, 2011, **134**, 041104.